INSTITUTE OF PHYSICS PUBLISHING COMBUSTION THEORY AND MODELLING

Combust. Theory Modelling **7** (2003) 221–242 PII: S1364-7830(03)53689-0

Effect of heat-loss on flame-edges in a premixed counterflow

R Daou, J Daou and J Dold

Department of Mathematics UMIST, Manchester M60 1QD, UK

E-mail: Joel.Daou@umist.ac.uk

Received 19 September 2002
Published 7 March 2003
Online at stacks.iop.org/CTM/7/221

Abstract

We describe the combined influence of heat-loss and strain (characterized here by non-dimensional parameters κ and ϵ, respectively) on premixed flame-edges in a two-dimensional counterflow configuration. The problem is formulated as a thermo-diffusive model with a single Arrhenius reaction. In order to help classify the various flame-edge regimes, the non-adiabatic one-dimensional problem which characterizes the wings (far downstream) of the flame-edge is briefly revisited and its solutions are delimited in the κ–ϵ plane. An analytical description of the flame-edges is then presented in the weak-strain limit $\epsilon \to 0$. This is complemented by a detailed numerical study. Several combustion regimes are found and their domains of existence are identified in the κ–ϵ plane. These include ignition fronts, extinction fronts, solutions with propagation speeds that depend non-monotonically on the strain-rate, propagating flame tubes and stationary flame tubes. Multiplicity of solutions and hysteresis phenomena, which are partly but not exclusively associated with the one-dimensional regimes, are also identified and discussed.

1. Introduction

Since the early work on triple-flames by Phillips [1] and Ohki and Tsuge [2], a great deal of information has been gathered on triple-flames, especially after the studies undertaken by Dold [3–5]. These flame structures, and their counterparts in premixed systems, can collectively be called 'flame-edges', denoting a region where some form of otherwise uniform flame structure comes to an end [6, 7]. Several aspects of flame-edges have been investigated over the last thirteen years or so, including gas-expansion effects, preferential-diffusion, proximity of cold surfaces and stability issues (see [8–17] and references therein). However, the influence of volumetric heat-losses on flame-edges seems to have received little attention in the published literature so far. A numerical study by Kurdyumov and Matalon [18] has considered the effects of volumetric heat-losses, which are found to provide a possible mechanism for

flame-edge oscillations in the non-strained mixing layer established at the mouth of a cylindrical injector.

In recent studies, we have investigated the effect of volumetric heat-loss, in some detail, both numerically [19] and analytically [20], in the non-premixed context of a triple-flame propagating in a strained mixing layer. In particular, we were able to obtain and to classify a number of different forms of triple-flame propagation, as well as the ranges of strain-rate and the rate of heat-loss for which they appear. The aim of this work is to carry out a similar investigation using the same basic two-dimensional counterflow configuration in premixed systems. Thus, we address the combined influence of strain and heat-loss on premixed flame-edges.

As will be seen, the results are far from a simple extension of the non-premixed case. In fact, a richer and more complex picture arises, associated with the existence of multiple solutions and hysteresis phenomena. The new complexities are partly, but not exclusively, related to the existence of multiple solutions of the underlying non-adiabatic one-dimensional problem (described, for example, in [21, 22]).

The paper is structured as follows. The problem is first formulated in a thermo-diffusive context with a single Arrhenius reaction. The one-dimensional problem, which can describe the trailing wings of a premixed flame-edge, far from the edge, is then revisited, since it is an essential prerequisite for understanding and classifying the two-dimensional results, which describe the flame-edge itself. An asymptotic analysis of flame-edge propagation under weak-strain conditions is then presented. This is followed by a numerical description of the general case, including a comparison with the asymptotic results and a synthesis of the various combustion regimes, by way of classifying the ranges of strain-rate and heat-loss intensity in which they can be found.

2. Formulation

The study is carried out in the counterflow configuration shown in figure 1, where the velocity field has components $v_X = 0$, $v_Y = -aY$ and $v_Z = aZ$ in the X-, Y- and Z-directions, respectively, measured dimensionally. Here, a is the strain-rate. We shall mainly address the steady propagation of premixed flame-edges along the X-axis, with their propagation speed $\hat{U}$ being positive if the fronts are moving in the negative X-direction. The chemistry will be represented by a one step irreversible Arrhenius reaction which consumes the fuel, considered to be deficient, at a rate $\hat{\omega} = \rho Y_{\mathrm{F}} B \exp(-E/RT)$, where B, ρ, Y_{F} and E/R represent the pre-exponential factor, the (constant) density, the mass fraction of fuel and the activation temperature, respectively.

In a reference frame attached to the flame, the governing equations are

$$\hat{U}\frac{\partial T}{\partial X} - aY\frac{\partial T}{\partial Y} = D_{\mathrm{T}}\left(\frac{\partial^2 T}{\partial X^2} + \frac{\partial^2 T}{\partial Y^2}\right) + \frac{q}{c_{\mathrm{p}}}\frac{\hat{\omega}}{\rho} - \hat{\kappa}(T - T_0), \tag{1}$$

$$\hat{U}\frac{\partial Y_{\mathrm{F}}}{\partial X} - aY\frac{\partial Y_{\mathrm{F}}}{\partial Y} = D_{\mathrm{F}}\left(\frac{\partial^2 Y_{\mathrm{F}}}{\partial X^2} + \frac{\partial^2 Y_{\mathrm{F}}}{\partial Y^2}\right) - \frac{\hat{\omega}}{\rho}. \tag{2}$$

Here, D_{T} and D_{F} are the thermal and mass diffusion coefficients. The term $\hat{\kappa}(T - T_0)$ is included in (1) to account for volumetric heat-losses in a simple way, the temperature in both incoming streams being T_0. The problem will be considered in the upper half-plane $Y \geqslant 0$, with boundary conditions (given in non-dimensional form below) corresponding to a frozen mixture as $X \to -\infty$ or $Y \to +\infty$, vanishing Y-derivatives at $Y = 0$ (because of symmetry) and vanishing X-derivatives as $X \to +\infty$.

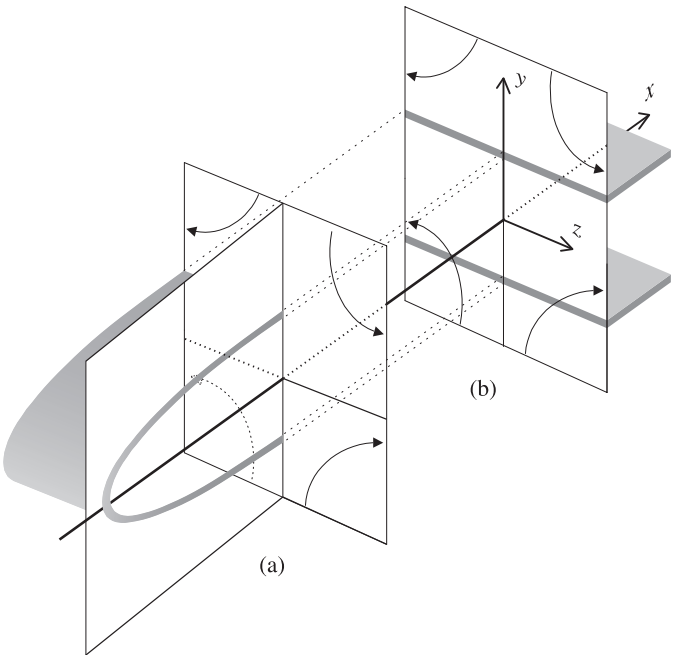

Figure 1. The counterflow configuration: (*a*) a two-dimensional flame-edge and (*b*) planar twin-flames.

For a non-dimensional formulation, we first introduce the scaled dependent variables

$$F \equiv \frac{Y_{\mathrm{F}}}{Y_{\mathrm{F,u}}} \qquad \text{and} \qquad \theta \equiv \frac{T - T_0}{T_{\mathrm{ad}} - T_0},$$

where $Y_{\mathrm{F,u}}$ is the composition in the frozen mixture and $T_{\mathrm{ad}} \equiv T_0 + qY_{\mathrm{F,u}}/c_{\mathrm{p}}$ is the adiabatic flame temperature. As unit speed, we select the laminar speed of the stoichiometric planar flame under adiabatic equidiffusional conditions, $S_{\mathrm{L}}^0 = [2\beta^{-2} D_{\mathrm{T}} B \exp(-E/RT_{\mathrm{ad}})]^{1/2}$, or more precisely its value in the asymptotic limit of large Zeldovich number $\beta \equiv E(T_{\mathrm{ad}} - T_0)/RT_{\mathrm{ad}}^2$. As unit length we select the (thermal) mixing layer thickness $L \equiv \sqrt{2D_{\mathrm{T}}/a}$.

In terms of the rescaled spatial coordinates $y \equiv Y/L$ and $x \equiv X/L$, we thus obtain the non-dimensional equations

$$U\frac{\partial\theta}{\partial x} - 2\epsilon y\frac{\partial\theta}{\partial y} = \epsilon\left(\frac{\partial^2\theta}{\partial x^2} + \frac{\partial^2\theta}{\partial y^2}\right) + \epsilon^{-1}\omega - \frac{\epsilon^{-1}}{\beta}\kappa\theta, \tag{3}$$

$$U\frac{\partial F}{\partial x} - 2\epsilon y\frac{\partial F}{\partial y} = \frac{\epsilon}{\mathrm{Le_F}}\left(\frac{\partial^2 F}{\partial x^2} + \frac{\partial^2 F}{\partial y^2}\right) - \epsilon^{-1}\omega. \tag{4}$$

The parameter ϵ is defined by

$$\epsilon \equiv \frac{l_{\mathrm{fl}}^0}{L} = \frac{l_{\mathrm{fl}}^0}{\sqrt{2D_{\mathrm{T}}/a}} \tag{5}$$

which represents the premixed flame thickness, $l_{\mathrm{fl}}^0 = D_{\mathrm{T}}/S_L^0$, measured against the reference length L. It is related to the Damköhler number, Da, by $\epsilon^{-2} = \mathrm{Da}$, if Da is defined as the ratio of the mechanical time, $2a^{-1}$, to the chemical reaction time $l_{\mathrm{fl}}^{0^2}/D_{\mathrm{T}}$. The parameter $\mathrm{Le_F} \equiv D_{\mathrm{T}}/D_{\mathrm{F}}$ is the Lewis number of the fuel, and $\kappa \equiv \beta(D_{\mathrm{T}}/S_{\mathrm{L}}^{0^2})\hat{\kappa}$ is the non-dimensional

heat-loss coefficient. The dimensionless reaction-rate ω is given by

$$\omega \equiv \frac{\beta^2}{2} F \exp \frac{\beta(\theta - 1)}{1 + \alpha_h(\theta - 1)}, \tag{6}$$

with $\alpha_h \equiv (T_{\rm ad} - T_0)/T_{\rm ad}$. The boundary conditions are

$$\theta = 0, \quad F = 1 \qquad \text{as } x \to -\infty \quad \text{or} \quad y \to \infty, \tag{7}$$

representing conditions in the frozen mixture, and

$$\frac{\partial \theta}{\partial x} = \frac{\partial F}{\partial x} = 0 \qquad \text{as } x \to \infty, \tag{8}$$

since the profiles are expected to be independent of x far downstream, and finally

$$\frac{\partial \theta}{\partial y} = \frac{\partial F}{\partial y} = 0 \quad \text{at} \quad y = 0, \tag{9}$$

for symmetry about $y = 0$.

In solving the problem above, the main aim is to determine the (scaled) propagation speed U in terms of the non-dimensional parameters ϵ, κ and $\mathrm{Le_F}$. This task will mainly be addressed numerically with the focus being on the dependence on the parameters ϵ and κ (characterizing the strain-rate and heat-loss intensity). Analytical results, valid in the weak-strain limit, will be also derived. However, as an essential prerequisite for the two-dimensional studies, the next section is dedicated to a review of the underlying one-dimensional problem.

3. The one-dimensional flame

The combined effect of strain and heat-loss on the planar premixed flame (the twin flames in figure 1) has been the subject of several studies in the literature (see, for example, [21, 22] and references therein). These studies have pointed out that typically two limits of extinction of the planar flame exist for a given intensity of the heat-loss: a 'quenching' limit at a high value of the strain-rate (as in the adiabatic case) and a 'radiation' limit at a lower value of the strain-rate. Although the reader is referred to the original publications for a detailed discussion of the problem, a succinct derivation of the main findings relevant to our study is provided here for convenience; the emphasis is on delimiting the different burning regimes in the κ–ϵ plane, which is not readily available in the literature.

An asymptotic approach, similar to that described in [22], is adopted using the limit $\beta \to \infty$ along with the nearly equidiffusive approximation $l_{\rm F} \equiv \beta(\mathrm{Le_F} - 1) = \mathrm{O}(1)$. The problem can then be reformulated in terms of the leading order temperature, θ^0, and the excess enthalpy $h \equiv \theta^1 + F^1$, where superscripts indicate orders of expansions in β^{-1}. More precisely, for $\beta \to \infty$, the chemical reaction is confined to an infinitely thin sheet located at $y = y_*$, say. On either side of this sheet, the equations

$$\frac{\mathrm{d}^2\theta^0}{\mathrm{d}y^2} + 2y\frac{\mathrm{d}\theta^0}{\mathrm{d}y} = 0,$$

$$\frac{\mathrm{d}^2 h}{\mathrm{d}y^2} + 2y\frac{\mathrm{d}h}{\mathrm{d}y} = -l_{\rm F}\frac{\mathrm{d}^2\theta^0}{\mathrm{d}y^2} + \kappa\epsilon^{-2}\theta^0,$$

must be satisfied along with the boundary conditions

$$\theta^0 = 0, \quad h = 0 \qquad \text{as } y \to \infty,$$

$$\frac{\mathrm{d}\theta^0}{\mathrm{d}y} = \frac{\mathrm{d}h}{\mathrm{d}y} = 0 \qquad \text{at } y = 0,$$

and the jump conditions

$$[\theta^0] = [h] = 0,$$

$$-\frac{1}{l_F}\left[\frac{dh}{dy}\right] = \left[\frac{d\theta^0}{dy}\right] = \epsilon^{-1}e^{\sigma/2},$$

at $y = y_*$. Here, σ stands for the perturbation in the flame temperature, $\sigma \equiv h(y_*)$ and, as is conventional, the squared bracket is equal to the value of a given quantity on the unburnt gas side (where $y = y_*^+$) minus its value at the burnt side ($y = y_*^-$).

Using the boundary conditions and the continuity of θ^0 and h at the reaction sheet, we thus find that

$$\theta^0 = 1,$$

$$h = \sigma - \frac{\kappa\sqrt{\pi}}{2\epsilon^2}\left([\mathrm{erf}(y_*) - \mathrm{erf}(y)]\int_0^{y_*} e^{u^2}\,du + \int_{y_*}^{y}[\mathrm{erf}(u) - \mathrm{erf}(y)]e^{u^2}\,du\right),$$

in the burnt gas region ($y < y_*$) and

$$\theta^0 = \frac{\mathrm{erfc}(y)}{\mathrm{erfc}(y_*)},$$

$$\begin{aligned} h = \sigma\frac{\mathrm{erfc}(y)}{\mathrm{erfc}(y_*)} + l_F\frac{y\exp(-y^2)\,\mathrm{erfc}(y_*) - y_*\exp(-y_*^2)\,\mathrm{erfc}(y)}{\sqrt{\pi}\,\mathrm{erfc}^2(y_*)} \\ - \frac{\kappa\sqrt{\pi}}{2\epsilon^2\mathrm{erfc}^2(y_*)}\left([\mathrm{erf}(y) - \mathrm{erf}(y_*)]\int_{y_*}^{\infty}\mathrm{erfc}^2(u)e^{u^2}\,du\right. \\ \left. +\mathrm{erfc}(y_*)\int_{y_*}^{y}[\mathrm{erf}(u) - \mathrm{erf}(y)]\,\mathrm{erfc}(u)e^{u^2}\,du\right), \end{aligned}$$

in the unburnt gas region ($y > y_*$).

It then follows from the jump conditions that the perturbation in the flame temperature σ and the location of the flame y_* are given in terms of ϵ, κ and l_F by

$$\begin{aligned} \sigma = & -\frac{\kappa\sqrt{\pi}}{2\epsilon^2\,\mathrm{erfc}(y_*)}\left[\mathrm{erfc}^2(y_*)\int_0^{y_*} e^{u^2}du + \int_{y_*}^{\infty}\mathrm{erfc}^2(u)e^{u^2}\,du\right] \\ & - \frac{l_F}{2}\left[1 + 2y_*^2 - \frac{2y_*\exp(-y_*^2)}{\sqrt{\pi}\,\mathrm{erfc}(y_*)}\right], \end{aligned} \tag{10}$$

$$\epsilon = \frac{\sqrt{\pi}}{2}\mathrm{erfc}(y_*)\exp\left(y_*^2 + \frac{\sigma}{2}\right). \tag{11}$$

For a fixed value of ϵ, equation (11) provides an explicit expression for σ in terms of y_* which when inserted in (10) yields an explicit formula for κ in terms of y_* and l_F. Thus, for fixed values of ϵ and l_F, a parametric plot of σ versus κ can be generated by varying y_* from zero to infinity.

Figure 2 summarizes the results for the unit Lewis number case $l_F = 0$. The dashed curves in this figure show the dependence of the burning rate per unit flame surface area $\mu \equiv \exp(\sigma/2)$ on κ, for selected values of ϵ. The inner solid curve, given by $\kappa = -\mu^2\ln(\mu)$, corresponds to the familiar non-adiabatic unstrained planar flame for which the lower branch is known to represent unstable solutions. Extinction here occurs at the turning point for which $\kappa = \kappa^0 \equiv (2e)^{-1}$. We note that this curve is approached by the dotted curves as ϵ (or the strain-rate) tends to zero, as is to be expected.

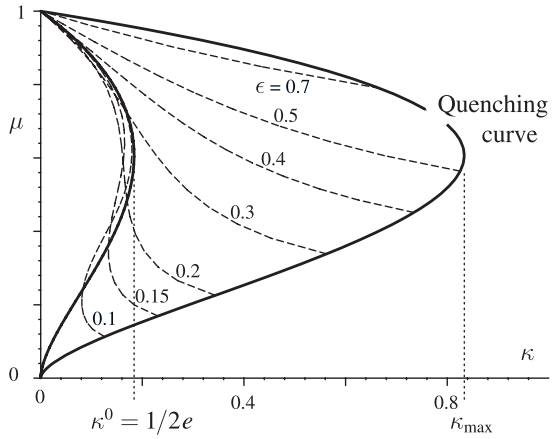

Figure 2. Burning rate per unit flame area versus κ for selected values of ϵ.

It can be seen that for any non-zero value of ϵ smaller than a critical value ϵ_c (which is found to be approximately equal to 0.186), the dotted curves are inverse-S-shaped curves indicating the existence of three burning solutions in a certain range of values of κ. It is reasonable to expect that the middle branch is unstable by analogy with the classical unstretched case; note anyway that this branch has the probably unphysical feature that the burning rate μ increases with κ. In addition to these three solutions, there is, of course, the frozen solution $\mu = 0$.

Thus, three stable planar solutions, including the frozen one, can be expected. It is seen, however, that at most one stable burning solution persists for any fixed value of κ in the asymptotic limit $\epsilon \to 0$, since the lower solution is then lost[1]. Furthermore, for $\epsilon > \epsilon_c$, μ becomes a monotonically decreasing single-valued function of κ, and flame extinction is obtained only by quenching at the stagnation plane.

The locus of the quenching points is the solid curve labelled 'quenching curve' obtained by setting $y_* = 0$ in (10) and (11). This curve shows that, in the presence of strain, burning solutions may be encountered for values of κ much larger than the planar extinction value $\kappa^0 \approx 0.184$, namely for $\kappa < \kappa_{\max}$, say. In fact, the locus of the quenching points in the κ–ϵ plane is described by the equation

$$\kappa = -\frac{4\epsilon^2}{A\sqrt{\pi}} \ln \frac{2\epsilon}{\sqrt{\pi}} \qquad \text{with } A \equiv \int_0^\infty \operatorname{erfc}^2(u) e^{u^2}\, \mathrm{d}u, \tag{12}$$

from which it can be deduced that $\kappa_{\max} = \sqrt{\pi}(2eA)^{-1} \approx 0.834$, corresponding to $\epsilon = \sqrt{\pi/4e} \approx 0.537$. Thus, the flame is most resistant to heat-loss for intermediate values of the strain-rate, namely for $\epsilon \approx 0.537$, being able to withstand a heat-loss intensity more than four times higher than the value that can be tolerated by a planar unstretched flame.

Another useful way of examining the results is by plotting μ as a function of ϵ for selected values of κ. Figure 3 summarizes the calculations obtained by solving the corresponding non-linear system for this (10) and (11) numerically. The quenching curve of the previous figure now appears as the straight line $\mu = 2\epsilon/\sqrt{\pi}$. Below this line no burning solutions can be obtained since they would correspond to negative values of y_*. The sections of the curves where, for fixed ϵ, the burning rate μ increases with κ, are almost certainly unphysical. These correspond to the middle branch of the inverse-S-shaped curves of the previous figure, and are shown dashed in figure 3. They appear here as the upper branch of the inverse-C-shaped curves

[1] This remark is important for the asymptotic study of the next section.

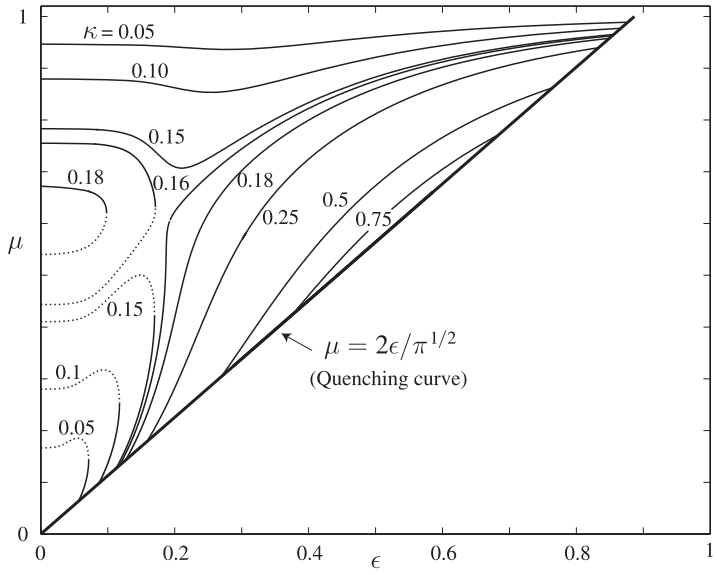

Figure 3. Burning rate per unit flame area versus ϵ for selected values of κ.

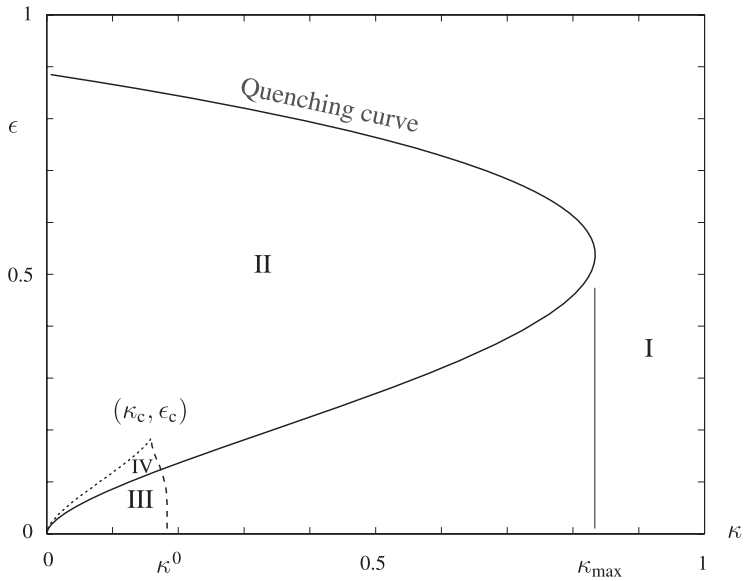

Figure 4. Parameter chart in the κ–ϵ plane.

in situations where $\kappa < \kappa_c \approx 0.159$. When $\kappa^0 > \kappa > \kappa_c$, they consist of the lower branch of the inverse-C-shaped curves. Note that for a fixed value of κ in the latter range, the ϵ-domain of existence of stationary solutions has a gap in it (see, for example, the case $\kappa = 0.18$).

Finally, figure 4 is a parameter plot, where regions characterizing the multiplicity of solutions in the κ–ϵ plane are identified. The solid curve in this diagram, labelled 'quenching curve,' is based on equation (12). The dashed and dotted curves, that anihilate each other in a cusp at (κ_c, ϵ_c), represent the loci of the upper and lower turning points, respectively. Thus,

based on the discussion above, four regions are delimited[2]. In region I, to the right of the quenching curve and of the dashed line, no burning solutions exist. In region II, to the left of the quenching curve and above the cusp, only one burning solution exists. In region III, inside the cusp and below the lower branch of the quenching curve, two burning solutions exist with the lower one being expected to be unstable. In the remaining small region IV, three burning solutions are found with the intermediate one being expected to be unstable. Of course, in all four regions we have, in addition, the frozen solution.

It is clear from this diagram that there are several possible ways in which two-dimensional travelling fronts, or flame-edges, can connect the various one-dimensional solutions above. In principle, any pair of solutions (of which the quenched solution is only one) can be connected by a stable or unstable flame-edge [6, 7]. However, in seeking only stable flame-edges, it must be stressed that the situation is simplified by the fact that only one stable burning solution is expected outside the small region IV. Although, several numerical calculations pertaining to region IV will be presented, much of our work will pertain to domains outside this region, which includes the domain pertinent to the asymptotic study of the next section corresponding to $\epsilon \to 0$ with κ fixed.

4. The weak-strain asymptotic limit

In the limit of weak-strain, $\epsilon \ll 1$, it is possible to describe the flame-edges analytically. The methodology is close to that used in [13, 20], and thus will be presented with less detail. We begin by reformulating the problem in the asymptotic limit $\beta \to \infty$ in the framework of the near-equidiffusion and near-adiabatic limit where l_F and κ are of order one, as in the previous section. We also rescale the problem by choosing as a new unit of length $2S_L^0/a$, leading to the new non-dimensional coordinates $\tilde{x} = \epsilon x$ and $\tilde{y} = \epsilon y$; this is the appropriate length-scale when considering small values of the strain-rate, since it is then equal, in order of magnitude, to the standoff distance of the twin-flames from the centreline. Characterizing the reaction sheet by the equation $\tilde{x} = f(\tilde{y})$, and introducing the flame-attached coordinate $\xi = \tilde{x} - f(\tilde{y})$, the resulting equations become

$$(U + 2\tilde{y}f')\frac{\partial\theta^0}{\partial\xi} - 2\tilde{y}\frac{\partial\theta^0}{\partial\tilde{y}} = \epsilon^2\Delta\theta^0, \tag{13}$$

$$(U + 2\tilde{y}f')\frac{\partial h}{\partial\xi} - 2\tilde{y}\frac{\partial h}{\partial\tilde{y}} = \epsilon^2\Delta h + \epsilon^2 l_F\Delta\theta^0 - \epsilon^{-2}\kappa\theta^0, \tag{14}$$

with

$$\Delta = (1 + f'^2)\frac{\partial^2}{\partial\xi^2} + \frac{\partial^2}{\partial\tilde{y}^2} - f''\frac{\partial}{\partial\xi} - 2f'\frac{\partial}{\partial\xi\partial\tilde{y}}.$$

The system (13) and (14) is to be solved for $\xi \neq 0$, subject to the jump conditions

$$\left[\theta^0\right] = [h] = 0, \tag{15}$$

$$\left[\frac{\partial h}{\partial\xi}\right] = -l_F\left[\frac{\partial\theta^0}{\partial\xi}\right], \tag{16}$$

$$\epsilon^2(1 + f'^2)^{1/2}\left[\frac{\partial\theta^0}{\partial\xi}\right] = \exp\left(\frac{\sigma}{2}\right), \tag{17}$$

[2] In regions I, II, III and IV there are 1, 2, 3 and 4 solutions respectively, including the frozen one.

at the reaction sheet located at $\xi = 0$. Here, $\sigma \equiv h(0, \tilde{y})$ is the value of h at $\xi = 0$. The boundary conditions are

$$\theta^0 = 0, \quad h = 0 \qquad \text{as } \xi \to -\infty \quad \text{or} \quad \tilde{y} \to \infty, \tag{18}$$

$$\frac{\partial \theta^0}{\partial \tilde{y}} = \frac{\partial h}{\partial \tilde{y}} = 0 \qquad \text{at } \tilde{y} = 0, \tag{19}$$

with the additional requirement that the solutions are to be free from exponentially growing terms as $\xi \to \infty$.

We now seek a perturbation solution to the reformulated problem (13)–(19), by writing expansions in the form

$$f = f_0 + \epsilon^2 f_1 + \cdots, \qquad U = U_0 + \epsilon^2 U_1 + \cdots,$$

with similar expressions for θ^0 and h. Note that only even powers of ϵ are considered since ϵ appears in its square in the equations. In the limit $\epsilon \to 0$, the flame, including its preheat zone, can be viewed as an infinitely thin layer located at $\xi = 0$, since its thickness is $O(\epsilon^2)$.

In the outer regions on both sides of the flame, it is readily found that

$$\theta^0 = \begin{cases} 0 & \text{for } \xi < 0, \\ 1 & \text{for } \xi > 0 \end{cases} \tag{20}$$

and

$$h = 0 \qquad \text{for } \xi < 0 \tag{21}$$

valid to all orders in ϵ. We shall not need the explicit form of the outer expansion of h downstream, since the exclusion of exponentially growing terms for $\xi > 0$, along with the matching with the outer solutions upstream, is sufficient to determine the inner solutions that we construct next.

We introduce the inner expansions

$$\theta^0 = \theta_0 + \epsilon^2 \theta_1 + \cdots, \qquad h = h_0 + \epsilon^2 h_1 + \cdots$$

and the stretched variable $\zeta \equiv \xi/\epsilon^2$. To leading order, this provides the equations

$$(U_0 + 2\tilde{y} f_0') \frac{\partial \theta_0}{\partial \zeta} = (1 + f_0'^2) \frac{\partial^2 \theta_0}{\partial \zeta^2}, \tag{22}$$

$$(U_0 + 2\tilde{y} f_0') \frac{\partial h_0}{\partial \zeta} = (1 + f_0'^2) \frac{\partial^2 h_0}{\partial \zeta^2} + l_F (1 + f_0'^2) \frac{\partial^2 \theta_0}{\partial \zeta^2} - \kappa \theta_0, \tag{23}$$

which describe the inner problem. These can be solved, using the jump conditions (15) and (16) and matching with the outer solutions, to give

$$\theta_0 = \begin{cases} \exp(\alpha \zeta) & \text{for } \zeta \leqslant 0, \\ 1 & \text{for } \zeta \geqslant 0, \end{cases} \tag{24}$$

$$h_0 = \begin{cases} -\left[\dfrac{2\kappa}{(\alpha (U_0 + 2\tilde{y} f_0'))} + \left(\alpha l_F - \dfrac{\kappa}{(U_0 + 2\tilde{y} f_0')} \right) \zeta \right] \exp(\alpha \zeta) & \text{for } \zeta \leqslant 0\,, \\ -\dfrac{2\kappa}{(\alpha (U_0 + 2\tilde{y} f_0'))} - \left(\dfrac{\kappa}{(U_0 + 2\tilde{y} f_0')} \right) \zeta & \text{for } \zeta \geqslant 0, \end{cases} \tag{25}$$

where

$$\alpha \equiv \frac{U_0 + 2\tilde{y} f_0'}{1 + f_0'^2}.$$

From (16), it then follows that

$$S_{L0} \exp\left(\frac{\kappa}{S_{L0}^2} \right) = 1,$$

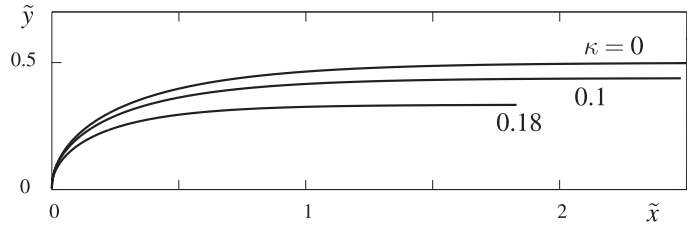

Figure 5. Asymptotic flame shape for selected values of κ.

where

$$S_{L0} \equiv \frac{U_0 + 2\tilde{y} f_0'}{(1 + f_0'^2)^{1/2}} \tag{26}$$

is the local laminar flame speed to leading order[3]. At the leading edge, we have $f_0' = 0$ and $S_{L0} = U_0$, so that

$$U_0 \exp\left(\frac{\kappa}{U_0^2}\right) = 1. \tag{27}$$

Thus, to leading order, S_{L0} and U_0 are equal to the propagation speed of the non-adiabatic planar flame. With these quantities being known, (26) can be reused to determine f_0', and thus the flame shape in the first approximation (see figure 5). Also, for later reference, we note that the flame curvature at the leading-edge, located at $y = 0$, is found to be

$$f_0''(0) = \frac{4}{U_0}. \tag{28}$$

At the next approximation the equations are

$$(U_0 + 2\tilde{y} f_0')\frac{\partial \theta_1}{\partial \zeta} - (1 + f_0'^2)\frac{\partial^2 \theta_1}{\partial \zeta^2} = \mathrm{L}(\theta_0) - (U_1 + 2\tilde{y} f_1')\frac{\partial \theta_0}{\partial \zeta} + 2\tilde{y}\frac{\partial \theta_0}{\partial \tilde{y}},$$

$$(U_0 + 2\tilde{y} f_0')\frac{\partial h_1}{\partial \zeta} - (1 + f_0'^2)\frac{\partial^2 h_1}{\partial \zeta^2} = \mathrm{L}(h_0 + l_\mathrm{F}\theta_0) - (U_1 + 2\tilde{y} f_1')\frac{\partial h_0}{\partial \zeta}$$
$$+ l_\mathrm{F}(1 + f_0'^2)\frac{\partial^2 \theta_1}{\partial \zeta^2} + 2\tilde{y}\frac{\partial h_0}{\partial \tilde{y}} - \kappa\theta_1, \tag{29}$$

where the operator L is given by

$$\mathrm{L} \equiv 2 f_0' f_1' \frac{\partial^2}{\partial \zeta^2} - f_0''\frac{\partial}{\partial \zeta} - 2 f_0'\frac{\partial^2}{\partial y \partial \zeta}. \tag{30}$$

These equations are valid for $\zeta \neq 0$. The jump conditions at $\zeta = 0$ are

$$[\theta_1] = [h_1] = 0, \qquad \left[\frac{\partial h_1}{\partial \xi}\right] = -l_\mathrm{F}\left[\frac{\partial \theta_1}{\partial \xi}\right],$$

$$\left[\frac{\partial \theta_1}{\partial \zeta}\right] = \left(\frac{\sigma_1}{2} - \frac{f_0' f_1'}{1 + f_0'^2}\right)\left[\frac{\partial \theta_0}{\partial \zeta}\right]. \tag{31}$$

[3] The laminar flame speed, $S_\mathrm{L} \sim S_{L0} + \epsilon^2 S_{L1}$, is given by $S_\mathrm{L} = (U\mathbf{i} - 2\tilde{y}\mathbf{j}) \cdot \mathbf{n}$ where the unit vector normal to the reaction sheet is $\mathbf{n} = (\mathbf{i} - f'\mathbf{j})/(1 + f'^2)^{1/2}$, pointing to the burnt gas; hence we have that $S_\mathrm{L} = (U + 2\tilde{y} f')/(1 + f'^2)^{1/2}$.

Downstream of the reaction sheet, it is found that θ_1 must be zero in order to be bounded as $\zeta \to \infty$ and to match with (20). We thus have from (29), after eliminating exponentially growing terms

$$\theta_1 = 0, \tag{32}$$

$$h_1 = \sigma_1 + \frac{\kappa\zeta}{(U_0 + 2\tilde{y}f_0')^2}(A + B\zeta) \qquad \text{for } \zeta \geqslant 0,$$

where

$$A = f_0'' - 4\frac{f_0'^2 + 3\tilde{y}f_0'f_0''}{U_0 + 2\tilde{y}f_0'} + U_1 + 2\tilde{y}f_1' + \frac{20\tilde{y}(1 + f_0'^2)(f_0' + \tilde{y}f_0'')}{(U_0 + 2\tilde{y}f_0')^2},$$

$$B = \frac{2\tilde{y}(f_0' + \tilde{y}f_0'')}{U_0 + 2\tilde{y}f_0'},$$

and σ_1 is as yet undetermined.

Solving for θ_1 in the unburnt gas, $\zeta \leqslant 0$, it is found that

$$\theta_1 = (C + D\zeta)\frac{\zeta \exp(\alpha\zeta)}{1 + f_0'^2}, \tag{33}$$

where

$$C = U_1 + 2\tilde{y}f_1' + f_0'' - 2f_0'f_1'\alpha + \frac{2\alpha'}{\alpha^2}\tilde{y} \qquad \text{and} \qquad D = f_0'\alpha' - \frac{\alpha'}{\alpha}\tilde{y},$$

after using the matching requirement $\theta_1 \to 0$ as $\zeta \to -\infty$, and the continuity requirement $\theta_1 = 0$ at $\zeta = 0$.

We now integrate equations (29) from $\zeta = -\infty$ to $\zeta = 0^-$ to obtain

$$\begin{aligned} &(1 + f_0'^2)\left[\frac{\partial\theta_1}{\partial\zeta}\right] = I_\theta - (U_1 + 2\tilde{y}f_1') - 2\tilde{y}\frac{\alpha'}{\alpha^2}, \\ &(U_0 + 2\tilde{y}f_0')\sigma_1 = I_h + l_F I_\theta + G \end{aligned} \tag{34}$$

after using (24), (25), (31) and (32), together with the matching condition that θ_1, h_1 and their derivatives with respect to ζ must vanish as $\zeta \to -\infty$. In (34), we have introduced the quantities

$$I_\theta = \int_{-\infty}^{0} \mathrm{L}(\theta_0)\,\mathrm{d}\zeta, \qquad I_h = \int_{-\infty}^{0} \mathrm{L}(h_0)\,\mathrm{d}\zeta$$

and

$$G = (1 + f_0'^2)\frac{\partial h_1}{\partial\zeta}\bigg|_{\zeta=0+} + (U_1 + 2\tilde{y}f_1')\sigma_0 + 2\tilde{y}\int_{-\infty}^{0}\frac{\partial h_0}{\partial y}\mathrm{d}\zeta - \kappa\int_{-\infty}^{0}\theta_1\,\mathrm{d}\zeta.$$

These can be evaluated from (24), (25) and (33), to give

$$I_\theta = 2f_0'f_1'\alpha - f_0'',$$

$$I_h = -2l_F f_0'f_1'\alpha + \frac{2\kappa(1 + f_0'^2)}{(U_0 + 2\tilde{y}f_0')^2}[f_0'' - f_0'f_1'\alpha]$$

and

$$\begin{aligned} G = &-2\tilde{y}\frac{\alpha'}{\alpha^2}l_F + \frac{\kappa(1 + f_0'^2)}{(U_0 + 2\tilde{y}f_0')^2}\bigg[2U_1 + 4\tilde{y}f_1' + A + C - \frac{2D}{\alpha} \\ &+ \frac{12\tilde{y}(1 + f_0'^2)}{(U_0 + 2\tilde{y}f_0')^2}\bigg[f_0' + yf_0'' + \frac{(U_0 + 2\tilde{y}f_0')\alpha'}{\alpha}\bigg]\bigg]. \end{aligned}$$

Now using the last jump condition of (31) in (34), we obtain a system of two equations for the three unknowns σ_1, U_1 and f_1'. However, it is possible to determine directly the perturbation in flame velocity, U_1, if the system of equations is applied at the leading edge of the flame, $y = 0$, where $f_0' = 0$. Thus, we obtain

$$U_1 = -f_0''(0)\left[1 + \frac{l_F}{2(1 - 2\kappa/U_0^2)}\right] = -\frac{4}{U_0}\left[1 + \frac{l_F}{2(1 - 2\kappa/U_0^2)}\right]. \tag{35}$$

At this stage, a two term approximation $U \sim U_0 + \epsilon^2 U_1$ is available for the propagation speed from (27) and (35). For example, for the case where $l_F = 0$ (to be considered in the numerical study below) we have

$$U \sim U_0 + \epsilon^2 U_1, \qquad \text{with } U_0 \exp\left(\frac{\kappa}{U_0^2}\right) = 1 \quad \text{and} \quad U_1 = -\frac{4}{U_0}. \tag{36}$$

A plot of U versus κ based on (36) will be given later, along with a comparison with numerical results (see figure 12).

5. Numerical results and discussion

In this section, numerical results corresponding to the problem (3)–(9) are presented. The numerical method used is based on a finite-volume discretization combined with an algebraic multigrid solver, as in [20]. The computational domain dimensions are typically 20 times the mixing layer thickness in the y-direction and 100 times the planar laminar flame thickness in the x-direction. The grid is non-uniform with typically 250 000 points. The results were calculated to describe the influence of ϵ and κ, with the other parameters being assigned fixed values, namely $\beta = 8$, $\alpha_h = 0.85$ and $\mathrm{Le_F} = 1$. The calculations are limited to $\epsilon > 0.1$ to ensure numerical accuracy.

We begin with a comparison between three cases, corresponding to $\kappa = 0$, $\kappa = 0.12$ and $\kappa = 0.2$, represented by figures 6, 7 and 8, respectively. In each case, five temperature contours are shown above and five reaction-rate contours are shown below, for selected values of ϵ increasing from left to right; in each figure, the largest values pertain to near-extinction conditions. The contours are equidistributed between zero and the maximum value indicated on each subfigure.

The adiabatic case $\kappa = 0$, corresponding to figure 6, shows a transformation of the flame-edge from an ignition-front propagating to the left with $U > 0$ (top subfigure) to an extinction-front retreating to the right with $U < 0$ (bottom subfigure). A similar behaviour is observed in figure 7 for a moderate value of κ, in which the reaction-rates are of course weaker, causing the transition from ignition to extinction fronts to occur at a lower value of ϵ. A notable qualitative new feature, however, which is absent when $\kappa = 0$, is the extinction of the trailing planar wings of the flame-edge, for small values of ϵ. For still larger values of κ, as illustrated in figure 8, the existence of ignition-fronts is no longer guaranteed, and the range of values of ϵ where flame-edge solutions are found is reduced.

The remarks just presented are supported and complemented by figure 9, where the propagation speed U is plotted against ϵ for selected values of κ. Disregarding, for the time being, the curve with triangles[4], we observe that the monotonic decrease of U from positive to negative values for moderate κ is similar to that encountered in the adiabatic case. However, when κ exceeds a critical value of the order of 0.13, a non-monotonic behaviour is obtained,

[4] The triangles represent another branch of weakly burning solutions. An example of such weakly burning solutions will be illustrated later in figure 17.

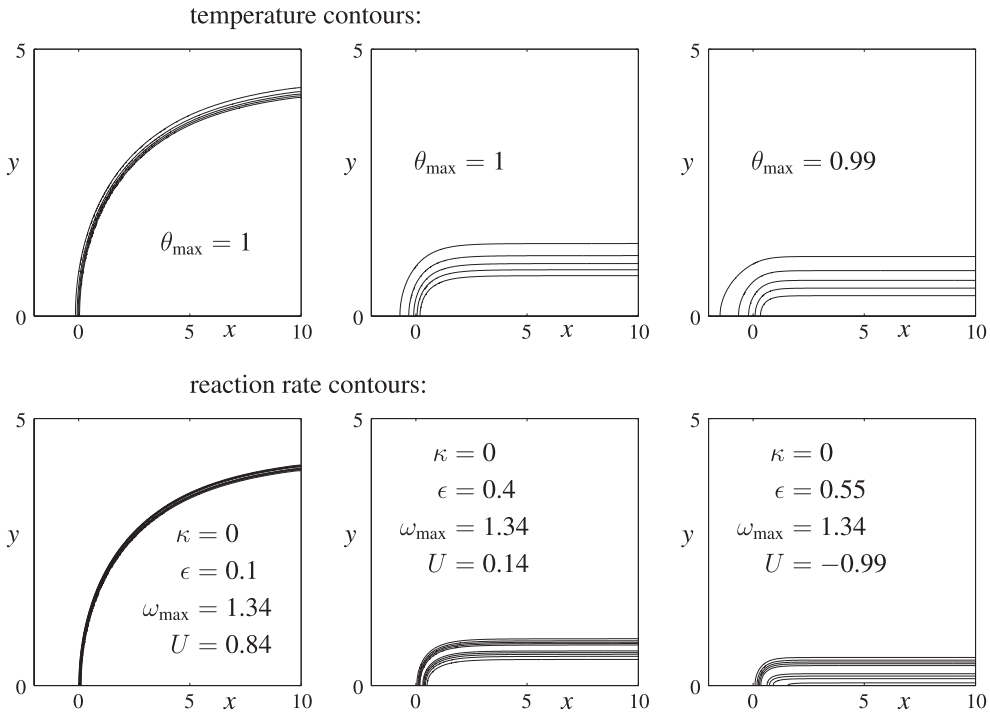

Figure 6. Reaction-rate and temperature contours.

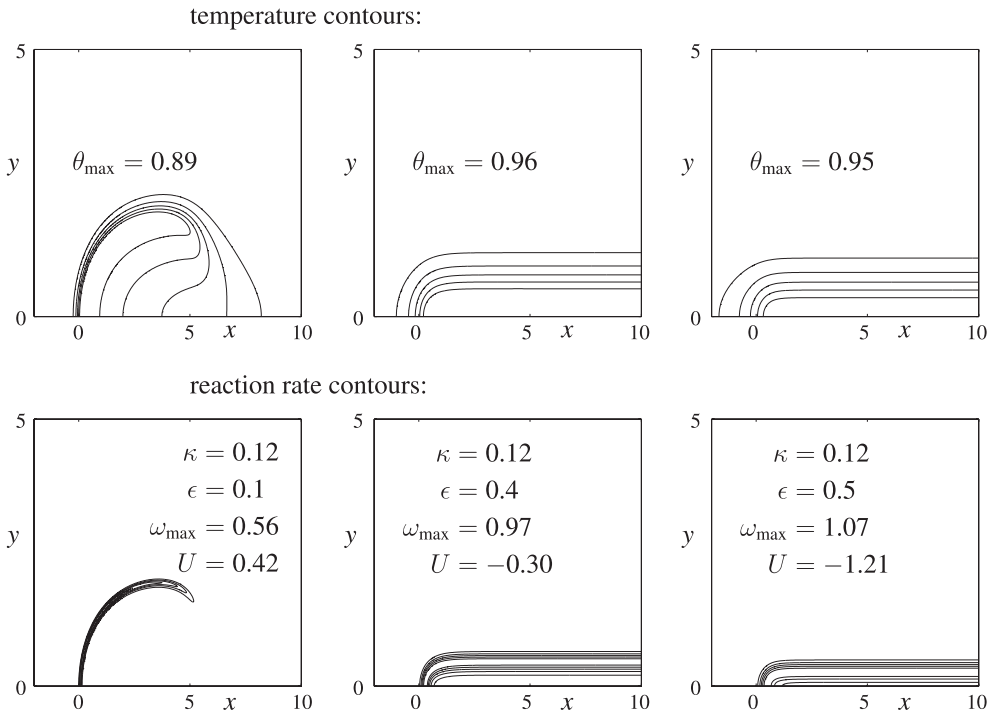

Figure 7. Reaction-rate and temperature contours.

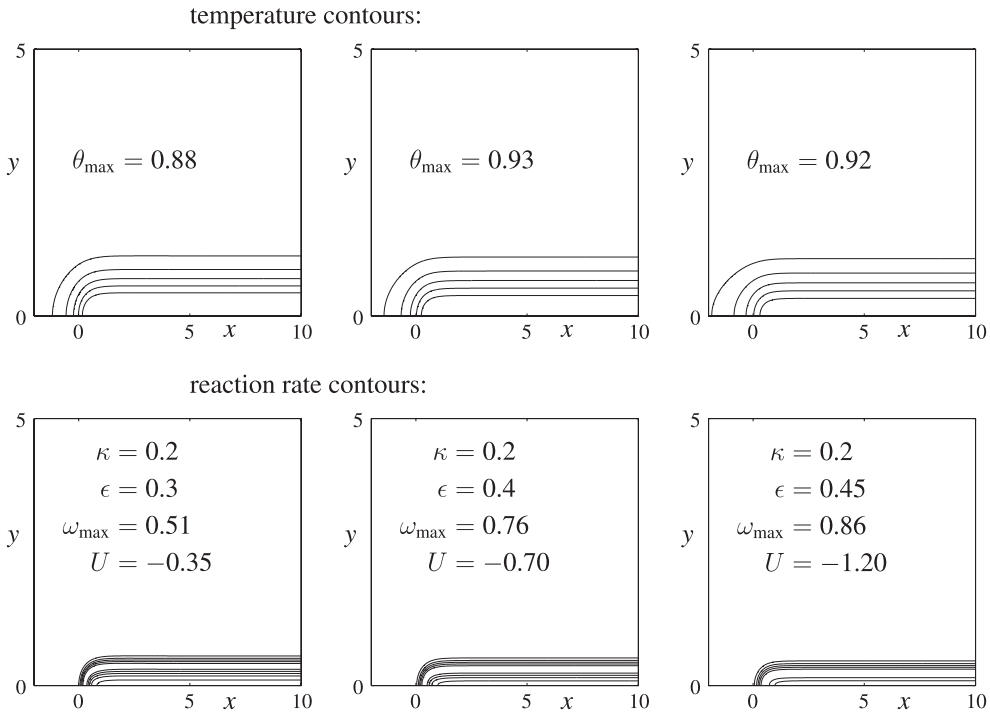

Figure 8. Reaction-rate and temperature contours.

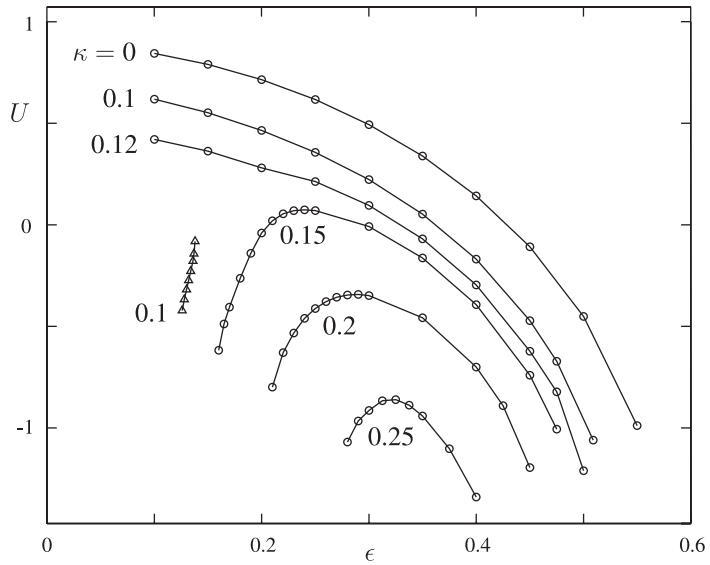

Figure 9. Propagation speed versus ϵ for selected values of κ.

and the ϵ-range of existence of the two-dimensional solutions is reduced; in particular, total extinction occurs at two values of ϵ (see, for example, the curve corresponding to $\kappa = 0.2$). The non-existence of two-dimensional burning solutions for such values of κ, when ϵ is sufficiently small, is explained by the asymptotic treatment of the previous section; as $\epsilon \to 0$, the flame

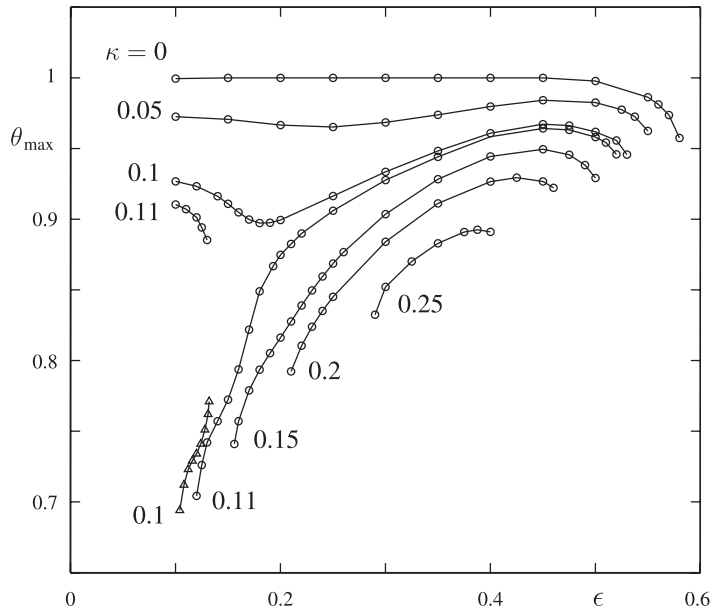

Figure 10. The planar strained flame.

tends locally to be a planar unstretched flame which does not exist when κ exceeds an extinction value[5].

The fact that the two-dimensional structure extinguishes at two values of the strain-rate is closely linked to the behaviour of the planar stretched flame. This can be seen from figure 10, where the maximum temperature of the planar flame is plotted against ϵ for selected values of κ. It is clear that this figure is consistent with figure 3 (based on asymptotics), although no attempt has been made here to obtain the physically dubious dashed branches of the latter. When κ has a small non-zero value, e.g. $\kappa = 0.10$, two solutions exist, with the strongly burning one extinguishing at a high value of ϵ, and the weakly burning one (with triangles) extinguishing at two lower values of ϵ. For larger values of κ, e.g. $\kappa = 0.20$, a unique burning solution is found with two extinction values of ϵ.

The influence of heat-loss at fixed values of ϵ is illustrated in figure 11 where the propagation speed U is plotted against κ. It is seen that under weak-strain conditions, such as $\epsilon = 0.1$, total extinction occurs at a finite positive speed, as in the case of a planar deflagration; this is not surprising since, as mentioned earlier, the flame front tends locally to be a planar deflagration as $\epsilon \to 0$. For larger values of ϵ, the two-dimensional structure experiences total extinction at a negative value of U.

A comparison between the asymptotic and numerical predictions of U as a function of κ is illustrated in figure 12, for the case $\epsilon = 0.1$. The asymptotic prediction is based on (36). The quantitative discrepancy observed can be attributed to the finite activation energy used in the computations. The numerically calculated value of κ at extinction, for $\beta = 8$, is simply lower than the asymptotic value for which $\beta \to \infty$. We can compare $\kappa_{\text{ext}}^{\text{num}} \approx 0.122$ with $\kappa_{\text{ext}}^{\text{asy}} \approx 0.184$. Also, in comparing the adiabatic values of U, corresponding to $\kappa = 0$, we find that $U_{\text{ad}}^{\text{num}} \approx 0.84$ and $U_{\text{ad}}^{\text{asy}} = 1 - 4\epsilon^2 \approx 0.96$. However, a linear rescaling of the numerical

[5] The theoretical extinction value, obtained in the limit $\beta \to \infty$, is $\kappa^0 = (2e)^{-1} \approx 0.184$. The numerical extinction value, obtained for $\beta = 8$, is $\kappa_{\text{num}}^0 \approx 0.125$.

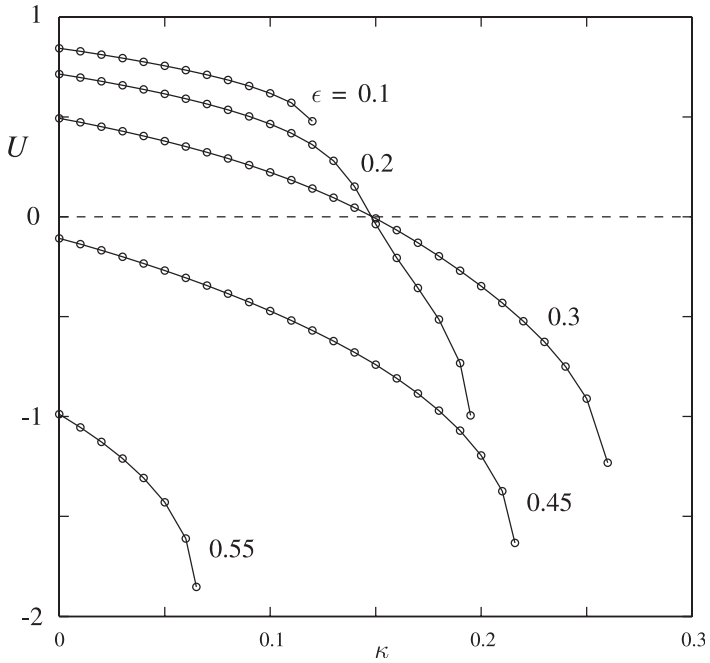

Figure 11. Propagation speed versus κ for selected values of ϵ.

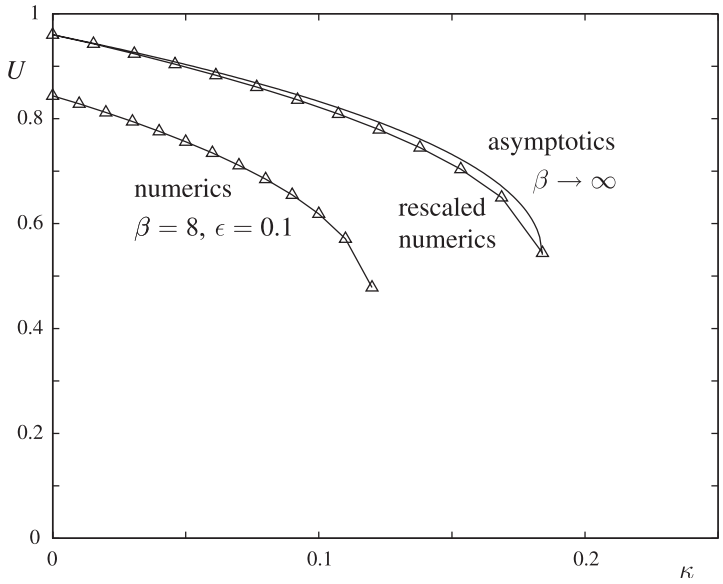

Figure 12. Comparison between asymptotic and numerical results.

results ($\kappa \mapsto \kappa\kappa_{\rm ext}^{\rm asy}/\kappa_{\rm ext}^{\rm num}$ and $U \mapsto UU_{\rm ad}^{\rm asy}/U_{\rm ad}^{\rm num}$) shows that the rescaled numerics compare rather well with the asymptotics, even under near-extinction conditions, as figure 12 shows.

The dependence of the flame shape on κ is illustrated in figure 13 for $\epsilon = 0.1$. Plotted are reaction-rate contours equidistributed between zero and the maximum value $\omega_{\rm max}$ indicated in each subfigure, as before. It is seen that the flame-front radius of curvature and its transverse

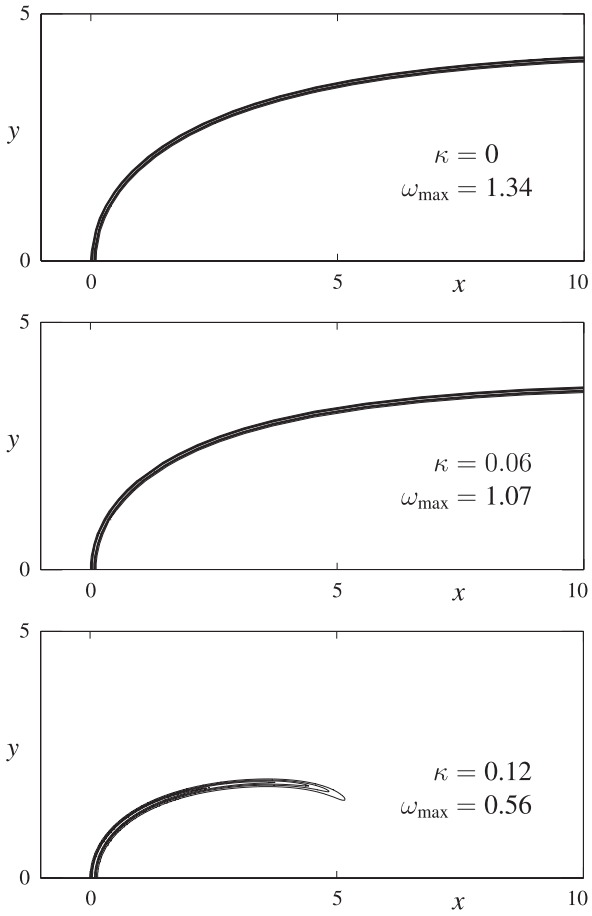

Figure 13. Reaction-rate contours for $\epsilon = 0.1$.

extent decrease with κ, in agreement with the analytical findings and with figure 5. Note also the extinction of the trailing wings of the flame-edge far downstream in the last subfigure.

A summary of the overall numerical findings discussed so far is provided by figure 14 in the κ–ϵ plane. The solid lines are deduced from one-dimensional numerical solutions; the inverse-C-shaped curve represents the locus of quenching points, and the curves forming a cusp represent the loci of the upper and lower turning points, as found numerically. The qualitative agreement with the asymptotic picture in figure 4 is clear. The squares correspond to the extinction limits of the two-dimensional flame-edges, and the triangles denote the conditions at which their propagation speed is zero. Since calculations could not be carried out accurately with $\epsilon < 0.1$, the dotted curves are extrapolations based on simply rescaling the corresponding asymptotic curves in figure 4.

Several regions are thus delimited. In the region labelled A, to the right of the squares, the flame-edge structures are entirely extinguished. The extinction in this case is dictated by the extinction of the planar structure in situations where the squares lie on the one-dimensional quenching curve. This occurs for ϵ larger than a critical value ϵ^* which is seen to be close to 0.13.

For smaller values of the strain-rate (more precisely for $\epsilon < \epsilon^*$), the two-dimensional flame structures can survive in situations where the planar flame is extinguished. This occurs in the

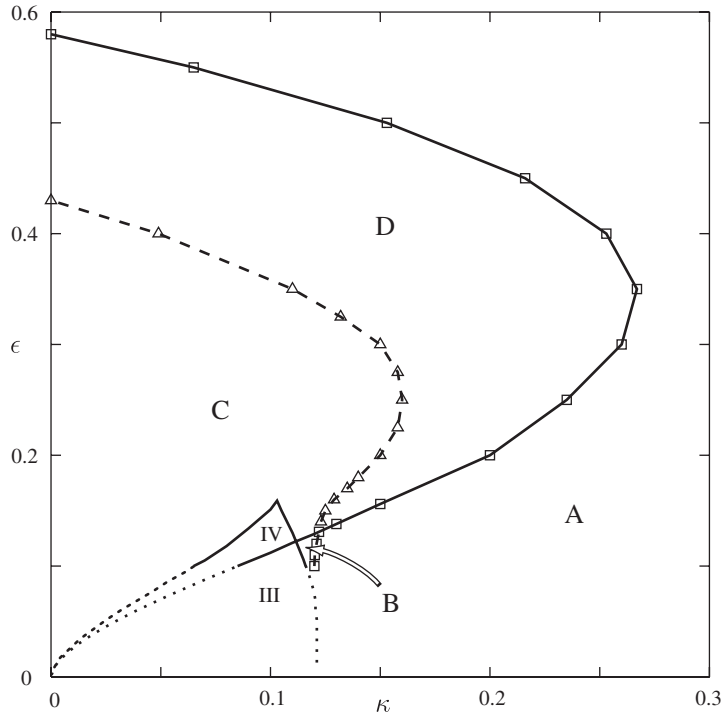

Figure 14. Regimes of flame-edge propagation under strain and heat loss.

region labelled B, where positively propagating flames without trailing wings are encountered, as seen in the top subfigures of figure 7.

These flame structures cannot accurately be described as flame-edges, since there is no flame of which they can form an edge. In a sense they are remnants of a flame-edge that has continued to survive in spite of the quenching of the flame of which they would otherwise have formed an edge; an analogous process at low Lewis numbers leads to oscillatory flame-edge propagation for both premixed and non-premixed systems [13–17]. It would be convenient to call these structures edge flames, since it is the edge-nature of the structure that clearly dominates, but this term has been used synonymously with flame-edges by some authors. They might be called isolated flame-edges. Analogous isolated flame-edge structures found in non-premixed systems have been termed tailless triple-flames [19, 20].

A non-propagating form of isolated flame-edge has also been identified in both premixed and non-premixed systems [14–17]. In [15, 16] these are called flame tubes. By extension, we might also therefore refer to the isolated flame-edges identified here, and in [19, 20] for the non-premixed case, as propagating flame tubes.

In the region labelled D, to the right of the triangles, retreating flame-edges are encountered. Finally, in the remaining region labelled C, including the regions III and IV, positively propagating flame-edges with infinite longitudinal extent are found. In region C we have, in addition to these, negatively propagating edges of flames correponding to the one-dimensional weakly burning solution; an example of such a flame is shown later in figure 17(*b*).

It should be emphasized that the rather extensive set of numerical simulations which are summarized in figure 14 is not exhaustive. Other complications arise whose detailed study may allow a more refined albeit more complex picture to be drawn. These complications are

mainly associated with the existence of multiple solutions and hysteresis phenomena and are briefly discussed in the remainder of this section.

A first example of multiplicity of solutions and hysteresis is illustrated in figures 15 and 16. Reaction-rate contours are plotted on the left and temperature contours are plotted on the right for a fixed value of κ, namely $\kappa = 0.12$. In figure 15, the profiles are obtained by starting from the initial solution corresponding to $\epsilon = 0.13$ and increasing ϵ. In figure 16, the profiles are obtained by starting from the initial solution corresponding to $\epsilon = 0.17$ and decreasing ϵ. Although the top and bottom subfigures are the same, the middle subfigures show two distinct solutions which are obtained for the same value of the parameters.

Another example of multiplicity of solutions is presented in figure 17, where three distinct solutions are shown for the same values of κ and ϵ. We first note that three one-dimensional solutions are obtained numerically in this case. In line with the analysis of section 3 these

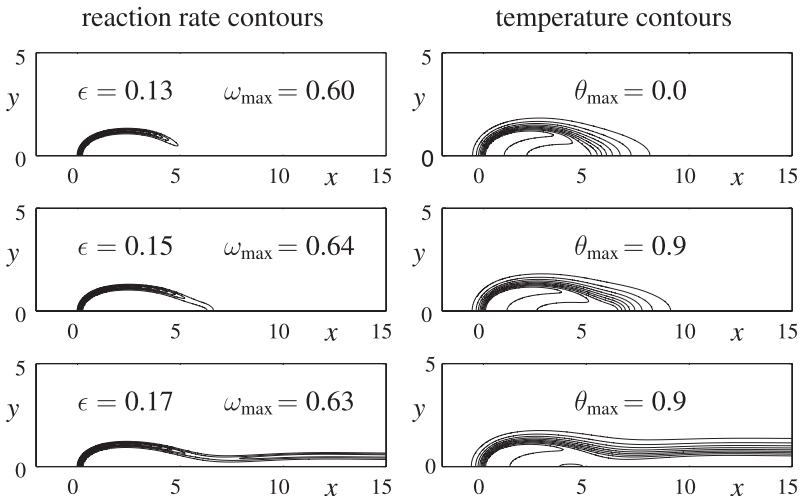

Figure 15. Reaction-rate and temperature contours.

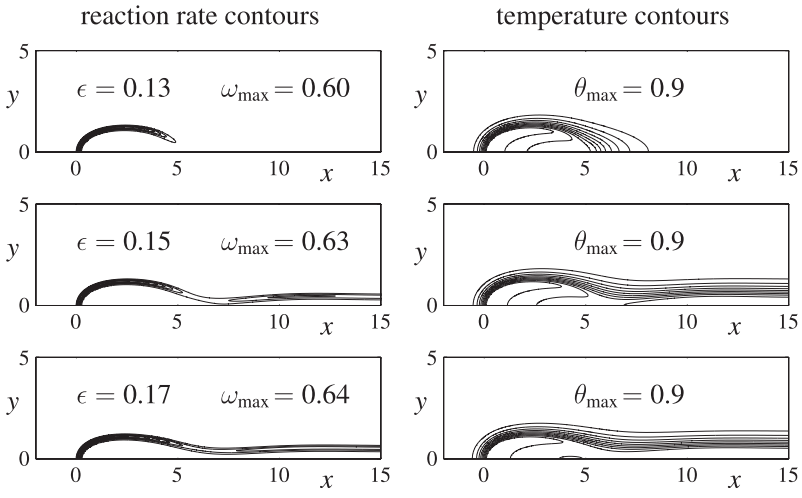

Figure 16. Reaction-rate and temperature contours.

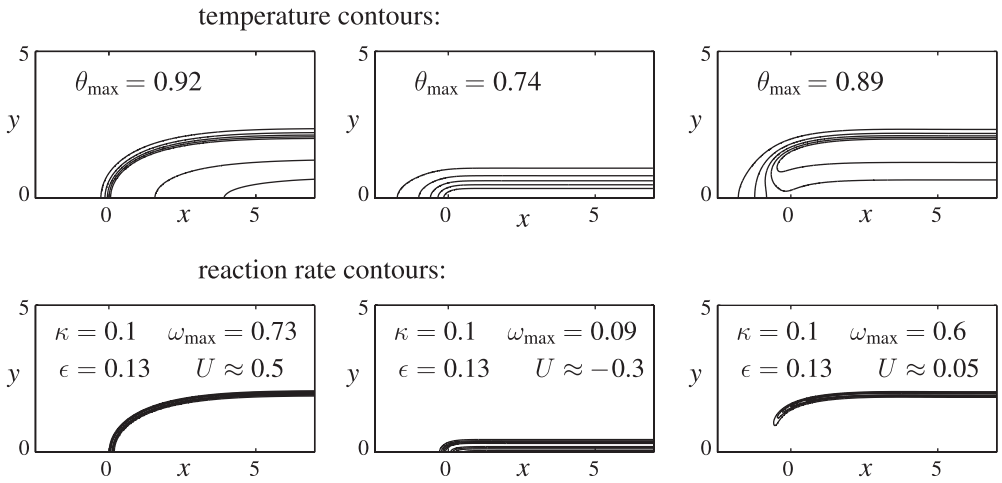

Figure 17. An example of multiple of solutions.

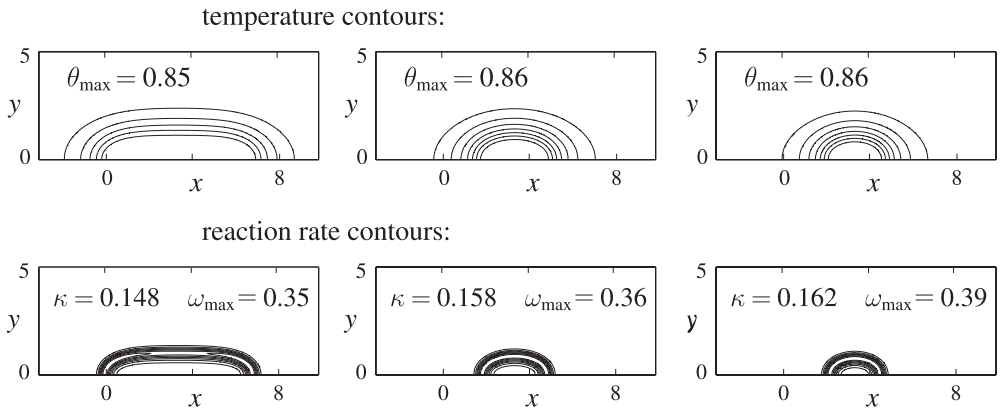

Figure 18. Reaction-rate and temperature contours with $\epsilon = 0.2$.

are: a frozen, a weakly burning, and a strongly burning solution. The left subfigures show a two-dimensional front connecting the frozen solution (far upstream) to the strongly burning one-dimensional solution (far downstream); the resulting propagation speed U (indicated on the subfigure) is positive. The middle subfigures show a two-dimensional front connecting the frozen solution to the weakly burning one-dimensional solution, with a resulting negative propagation speed. The right subfigures show another two-dimensional front connecting the frozen solution to the strongly burning one-dimensional solution, with a small negative value of U [6].

Yet another type of solution which has not been considered so far corresponds to stationary flame tubes (for which $U = 0$). Examples of these are shown in figure 18. Reaction-rate and temperature contours are plotted for $\epsilon = 0.2$ and three values of κ increasing from left to right. It can be seen that the size of the tube decreases with increasing κ. The longitudinal extent of these tubes, as a function of κ, is shown in figure 19 for selected values of ϵ. For each value

[6] We have not been able to find a two-dimensional front connecting the weakly and strongly burning solutions to each other. It may be possible that no travelling wave solution (with constant U) exists which may achieve this connection.

of ϵ, the tubes exist between two critical values of κ. As κ is increased above the upper value the tube is extinguished, while as κ approaches the lower value, the longitudinal extent of the tube approaches infinity, tending to regenerate the planar structure.

Finally, it is instructive to delimit the existence domains of the stationary and non-stationary tubes in the κ–ϵ plane. This is carried out in figure 20. The squares and triangles in this figure have the same meaning as in figure 14 and are included here for reference. It is seen that the domains of existence of the stationary and non-stationary tubes are not disjoint. This illustrates once more the frequent occurrence of multiple two-dimensional solutions, and

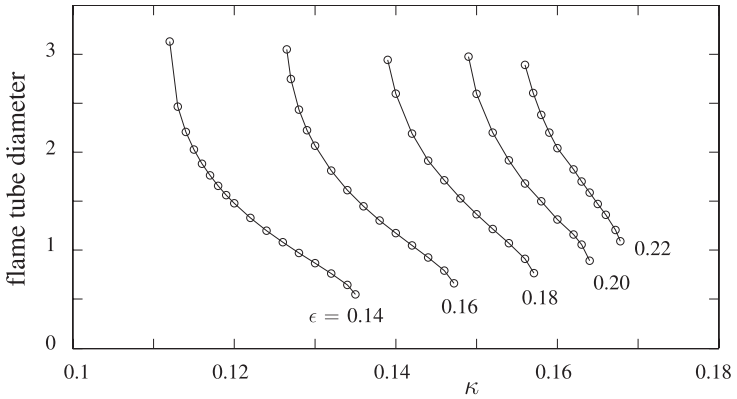

Figure 19. Longitudinal extent of stationary tubes versus κ for selected values of ϵ.

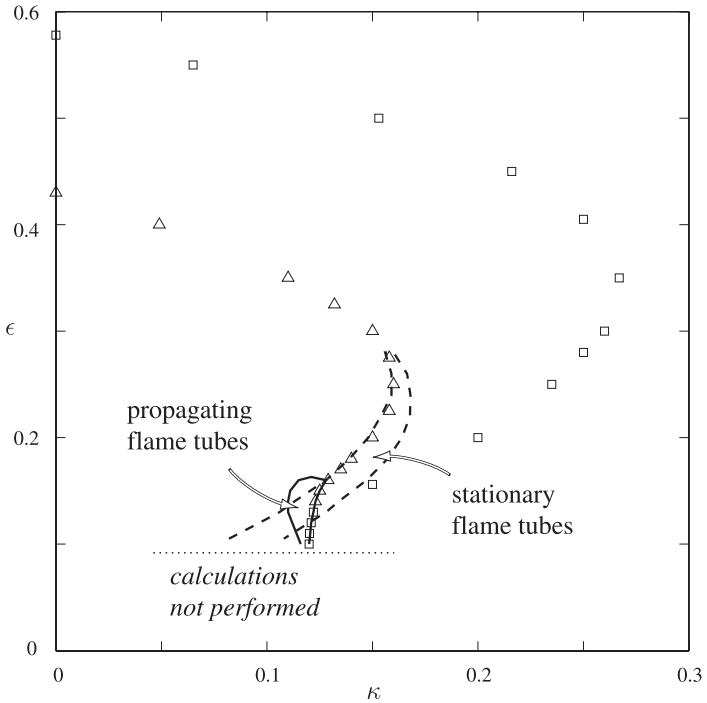

Figure 20. Existence domains of stationary and propagating tubes.

emphasizes that this added complexity is not necessarily related to that of the underlying one-dimensional problem.

6. Conclusion

Two-dimensional flame-edges, isolated flame-edges or propagating flame tubes and non-propagating flame tubes, encountered in a premixed counterflow configuration under non-adiabatic conditions have been investigated analytically in the weak-strain and large activation energy limits, and numerically for a finite activation energy. The results illustrate the existence of a wide spectrum of behaviour, which we have discussed and classified in a two-dimensional diagram characterizing the rates of heat-loss and strain. The complexity of the problem has been associated in part with the existence of multiple solutions of the underlying one-dimensional y-dependent problem. However, other issues which are not directly related to the one-dimensional problem, such as the coexistence of stationary and propagating tubes and the multiplicity of two-dimensional travelling-wave solutions with the same conditions far upstream and downstream, have also arisen. A natural extension of the present work, which is worth undertaking, is to account for unsteady effects and to study the stability of the various stationary solutions presented. A non-linear radiative heat-loss term could also be considered, as in [18]. However, even without these additional aspects, the present work constitutes an important first step in uncovering the effect of heat-loss on premixed flame-edges.

Acknowledgments

The authors are grateful to the EPSRC for financial support.

References

[1] Phillips H 1965 *Proc. Combust. Inst.* **10** 1277
[2] Ohki Y and Tsuge S 1986 *Prog. Astronaut. Aeronaut.* **105** 233
[3] Dold J W 1988 *Prog. Astronaut. Aeronaut.* **113** 240–8
[4] Dold J W 1989 *Combust. Flame* **76** 71–88
[5] Hartley L J and Dold J W 1991 *Combust. Sci. Technol.* **80** 23
[6] Dold J W 1997 *Prog. Astronaut. Aeronaut.* **173** 61–72
[7] Dold J W 2002 *Nonlinear PDEs in Condensed Matter and Reactive Flows* ed H Berestycki and Y Pomeau (Dordrecht: Kluwer) pp 99–113
[8] Liñán A 1994 *Combustion in High Speed Flows* ed J Buckmaster, T L Jackson and A Kumar (Boston: Kluwer) p 461
[9] Kioni P N, Rogg B, Bray C and Liñán A 1993 *Combust. Flame* **95** 276–90
[10] Buckmaster J and Matalon M 1989 *Proc. Combust. Inst.* **22** 1527–35
[11] Ruetsch G R, Vervisch L and Liñán A 1995 *Phys. Fluids* **7** 1447–54
[12] Wichman I S 1999 *Combust. Flame* **384** 384
[13] Daou J and Liñán A 1998 *Combust. Theory Modelling* **2** 449–77
[14] Daou J and Liñán A 1999 *Combust. Flame* **118** 479–88
[15] Shay M L and Ronney P D 1998 *Combust. Flame* **112** 171
[16] Thatcher R W and Dold J W 2000 *Combust. Theory Modelling* **4** 435–57
[17] Thatcher R W, Omon-Arancibia A and Dold J W 2002 *Combust. Theory Modelling* **6** 487–502
[18] Kurdyumov V and Matalon M *Proc. Combust. Inst.* **29** 45–52
[19] Daou R, Daou J and Dold J *Proc. Combust. Inst.* **29** 1559–64
[20] Daou R, Daou J and Dold J The effect of heat loss on flame edges in a nonpremixed counterflow (submitted)
[21] Sung C J and Law C K 1997 *Proc. Combust. Inst.* **26** 865
[22] Buckmaster J 1997 *Combust. Theory Modelling* **1** 1
[23] Liu F, Smallwood G J, Gülder Ö L and Ju Y 2000 *Combust. Flame* **121** 275–87
[24] T'ien J S 1982 *Combust. Flame* **65** 31–4
[25] Chao B H, Law C K and T'ien J S 1991 *Proc. Combust. Inst.* **23** 523